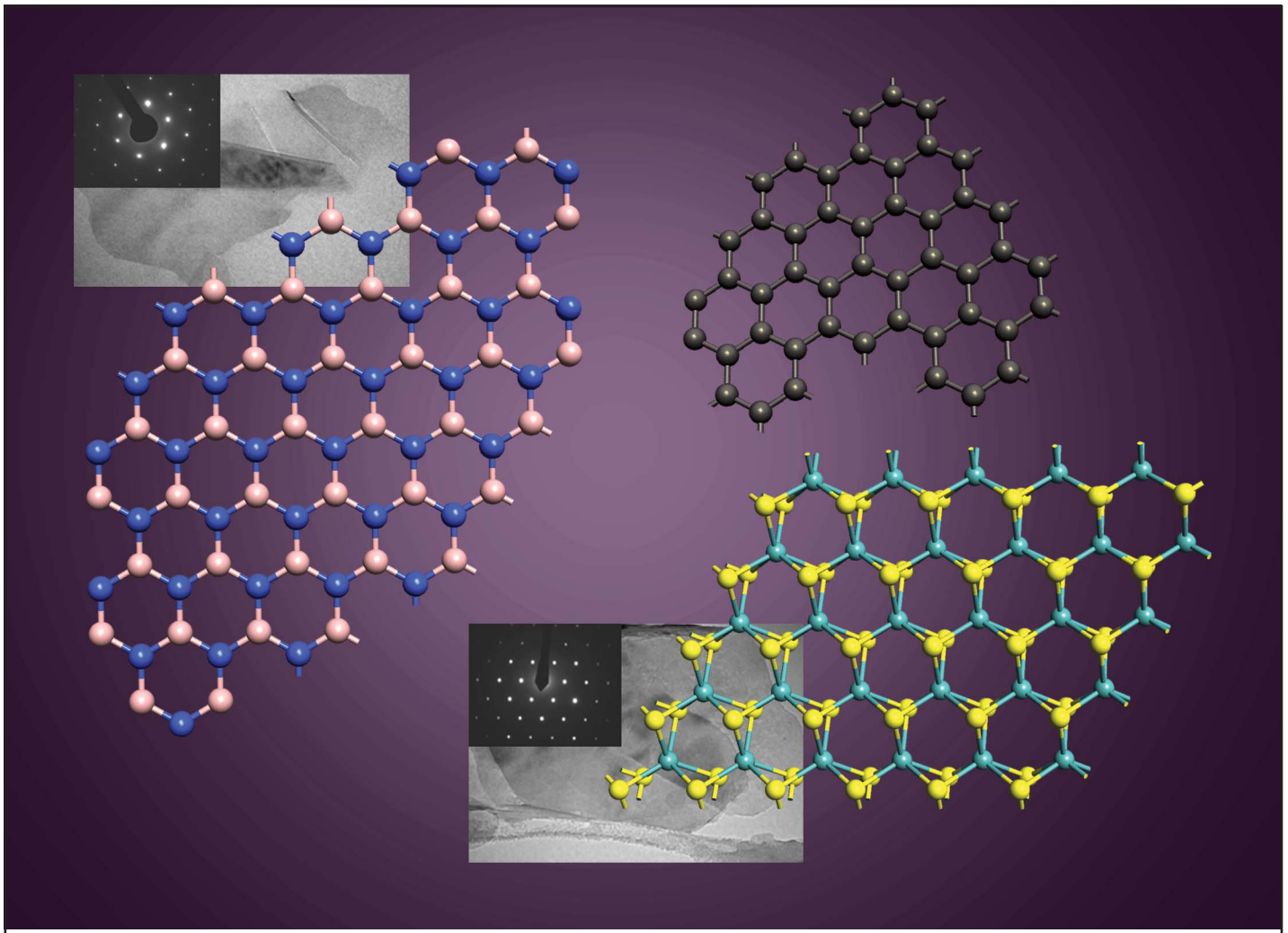

Highlighting research results from Y. G. Yao, X. J. Song and C. P. Wong *et al*., Georgia Technology Research Institute, Georgia Institute of Technology.

Title: Large-scale production of two-dimensional nanosheets

We report a facile method for the fabrication of monolayer and few-layer BN, MoS_2, and graphene using combined ball milling and sonication, and application of these nanosheets toward gas sensing.

As featured in:

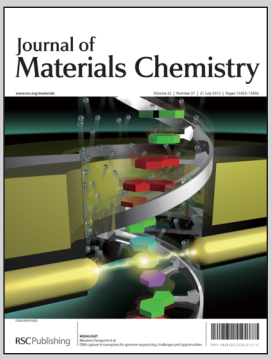

See Yagang Yao *et al.*, *J. Mater. Chem*., 2012, **22**, 13494.

RSC Publishing

www.rsc.org/materials

Registered Charity Number 207890

Journal of Materials Chemistry

Dynamic Article Links

Cite this: J. Mater. Chem., 2012, 22, 13494

www.rsc.org/materials

PAPER

Large-scale production of two-dimensional nanosheets†

Yagang Yao,[a] Ziyin Lin,[a] Zhuo Li,[a] Xiaojuan Song,[b] Kyoung-Sik Moon[a] and Ching-ping Wong*[ac]

Received 31st January 2012, Accepted 4th April 2012
DOI: 10.1039/c2jm30587a

Two-dimensional (2D) nanomaterials such as graphene, boron nitride (BN), and molybdenum disulfide (MoS_2) have been attracting increasing research interest in the past few years due to their unique material properties. However, the lack of a reliable large-scale production method is an inhibiting issue for their practical applications. Here we report a facile, efficient, and scalable method for the fabrication of monolayer and few-layer BN, MoS_2, and graphene using combined low-energy ball milling and sonication. Ball milling generates two forces on layered materials, shear force and compression force, which can cleave layered materials into 2D nanosheets from the top/bottom surfaces, and the edge of layered materials. Subsequent sonication would further break larger crystallites into smaller crystallites. These fabricated 2D nanosheets can be well dispersed in aqueous solutions at high concentrations, 1.2 mg mL^{-1} for BN, 0.8 mg mL^{-1} for MoS_2, and 0.9 mg mL^{-1} for graphene, which are highly advantageous over other methods. These advantages render great potential in the construction of high-performance 2D material-based devices at low cost. For example, a prototype gas sensor is demonstrated in our study using graphene and MoS_2, respectively, which can detect several ppm of ammonia gas.

Introduction

Since the discovery of graphene, various two-dimensional (2D) nanosheets such as transition metal dichalcogenides (TMDs, *e.g.* MoS_2 and WS_2), transition metal oxides (TMOs), and hexagonal boron nitride (h-BN) have been attracting intensive attention due to the unusual properties associated with their ultrathin structure.[1–31] For example, graphene, a single layer of carbon atoms bonded together in a hexagonal lattice, has large specific surface area (2630 $m^2\ g^{-1}$), large Young's modulus (1100 GPa), high charge carrier mobility (~200 000 $cm^2\ V\ s^{-1}$), and high thermal conductivity (~5000 W mK^{-1}).[27–31] h-BN, the so-called "white graphene", has high temperature stability, large band gap (electrically insulting), low dielectric constant (4.6), high hardness (15–24 kg mm^{-2}), high corrosion resistance, and large thermal conductivity (~6600 W mK^{-1}).[13–20] Monolayer MoS_2, distinct from its bulk form, is a direct band gap semiconductor with a band gap of 1.8 eV, and has a high fluorescence yield.[2–5,7,9,10] These unique properties make them promising candidates for wide applications in electronics, sensors, catalysis, photovoltaics, energy storage devices, *etc.*[1–5,7,10,14–16,18,22–31]

Top-down exfoliation from stacked three-dimensional (3D) crystals is a commonly used method to prepare these 2D materials. Micromechanical cleavage by Scotch tape is the first method for mechanical fragmentation of layered materials into individual 2D nanosheets, and has been used to prepare graphene, h-BN, and MoS_2.[1–3,5,7,10] Although this method provides high quality 2D nanosheets, the extremely low yield is a critical problem. Another method for high volume production of graphene is by the reduction of graphite oxide (GO) sheets.[32,33] However, this method is not applicable to other stable layered materials such as h-BN. The intercalation of various intercalates (*e.g.* alkali metals, large or long organic solvents, and transition-metal halides) is another useful method for the exfoliation of the intercalated compounds.[34–38] However, this method is very sensitive to the environmental conditions and the removal of intercalates results in the re-aggregation of layered materials. Furthermore, incomplete ion insertion can lead to a low yield at exfoliation while over-intercalation of ion results in structural deformations in some TMDs. Recently, Zeng *et al.* have demonstrated a controllable lithium intercalation process *via* incorporation of layered bulk materials, such as MoS_2, WS_2, TiS_2, TaS_2, ZrS_2, and graphite, as the cathode in an electrochemical set-up.[6] However, the complicated electrochemical process may limit its applications. Hence, it is desirable to develop a new strategy to produce 2D nanosheets on a large scale in order to realize their practical applications.

[a]*School of Materials Science and Engineering, Georgia Institute of Technology, 771 Ferst Drive NW, Atlanta, GA 30332, USA. E-mail: cp.wong@mse.gatech.edu; Fax: +1 404 894 9140; Tel: +1 404 894 8391*
[b]*Electro-Optical System Lab, Georgia Technology Research Institute, Georgia Institute of Technology, 925 Dalney Street NW, Atlanta, GA 30332, USA*
[c]*Department of Electronic Engineering, Faculty of Engineering, The Chinese University of Hong Kong, ShaTin, Hong Kong, People's Republic of China*

† Electronic supplementary information (ESI) available: Additional figures. See DOI: 10.1039/c2jm30587a

Liquid-phase exfoliation of layered materials has been found to have great potential for the scalable production of 2D nanosheet-based materials, such as 2D nanosheet suspensions, thin films by vacuum filtration, and 2D nanosheet-based hybrids and composites.[12,39] Coleman *et al.* have shown that layered materials such as MoS_2, WS_2, $MoSe_2$, $MoTe_2$, $TaSe_2$, $NbSe_2$, $NiTe_2$, BN, and Bi_2Te_3 can be exfoliated to monolayer and few-layer 2D nanosheets in various organic solvents *via* sonication.[12] However, the concentrations of the resulting MoS_2, WS_2, and BN suspensions are only 0.3, 0.15, and 0.06 mg mL^{-1}, respectively, which are still low for large-scale applications. In addition, the solvents used are expensive and toxic, requiring special care during handling, and have high boiling points, which makes them difficult to remove. Later, they reported an improved exfoliation method in an aqueous surfactant solution *via* high power tip sonication. But the concentration they could achieve (around 0.25 mg mL^{-1} for MoS_2) is still not high enough.[11] Zhou *et al.* recently reported that a mixed-solvent, ethanol–water at an appropriate ratio, can be used to exfoliate inorganic graphene analogues such as BN and MoS_2.[39] In spite of the low cost, the concentrations of 0.018 mg mL^{-1} for MoS_2, 0.032 mg mL^{-1} for WS_2, and 0.075 mg mL^{-1} for BN achieved are still low.

The liquid exfoliation process generally involves two steps: the thinning of layered materials into small individual 2D nanosheets, and then further dispersion of these nanosheets in solvents. In order to achieve efficient exfoliation of layered materials, the thinning method needs to be efficient and scalable, and cause less damage to layers of the materials. The solvents used for dispersion are required to be capable of preventing the aggregation of 2D nanosheets driven by their high surface energy. Moreover, it would be better if the solvents are volatile (easy to be removed), cheap, and eco-friendly. However, previous work on liquid exfoliation of layered materials are more focused on how to disperse and stabilize the exfoliated 2D materials while less attention has been paid on how to optimize the thinning process to improve the scalability. Herein, we report a combined low-energy ball milling and sonication procedure for the thinning and exfoliation of layered materials on a large scale. We have tailored the time of low-energy ball milling, and the combination of low-energy ball milling and sonication to produce high concentrations of 2D nanosheets—1.2 mg mL^{-1} for BN, 0.8 mg mL^{-1} for MoS_2, and 0.9 mg mL^{-1} for graphene. Few-layer and monolayer BN, MoS_2, and graphene are achieved in surfactant sodium dodecyl sulfate (SDS)–water solutions, which are ready for large-scale applications. The results show that the ionic surfactant SDS is a cheap and nice stabilizer to prevent 2D nanosheets from aggregating. We also demonstrate that this approach is very useful in the construction of high-performance 2D materials-based devices at low cost, for instance, in ammonia gas sensing.

Experimental

2D materials preparation and characterization

h-BN and graphite flakes were supplied by Momentive and Asbury Carbon, respectively. MoS_2 and SDS were purchased from Sigma-Aldrich. All chemicals were used as received. A horizontal planetary mill (Labmill-8000) and a sonicator (Misonix 3000) were used for thinning of layered materials. The initial powders, 2.0 g h-BN, MoS_2 or graphite, and 200 mL 0.05 weight% SDS–water were loaded in a sealed polyethylene wide-mouthed bottle with 200 zirconia balls (2 mm in diameter). The rotation speed of the planetary mill was set at 100 rpm to generate rolling actions of the balls which apply shearing forces on materials. 20 mL of milled samples were taken out after milling for various durations (1, 3, 6, and 12 h) for analyses, followed by centrifugation at 5000 rpm for 20 minutes to remove aggregates. After that, h-BN, MoS_2, and graphene supernatants were achieved. For 12 h ball milling samples, an additional 2 h of sonication at low power output (80 W) was applied to further exfoliate layered materials. To determine the concentrations of 2D nanosheets in the supernatant, two methods were used. In the first method we measured the weight of 2D nanosheets in 1 mL of supernatant in a microbalance, assuming that SDS gets distributed uniformly within the supernatant. 1 mL of solution was taken out from the supernatant, and then the average mass of 2D nanosheets in 1 mL of supernatant was weighed after drying the water in a vacuum oven at 120 °C and subtracting the mass of the surfactant SDS. Totally 10 mL of the supernatant were examined for each sample. In the second method we measured the weight of 2D nanosheets in 200 mL of supernatant. 200 mL of the supernatant was filtered and a large amount of hot water was used to wash the SDS away. The weight of 2D materials within 200 mL supernatant was measured with the microbalance after drying the water in a vacuum oven at 120 °C. Transmission electron microscopy (TEM) images were obtained using JEOL TEM 100CX and Hitachi TEM HF 2000. Atomic force microscopy (AFM) images were achieved using a Dimension 3100 scanning probe microscope. The morphologies of 2D nanosheets were obtained using scanning electron microscopy (SEM, JEOL 1530 and 1550). Because of the weak contrast caused by the very thin nanosheets and their insulating electrical properties, the vacuum filtrated films and 2D nanosheets deposited on SiO_2 substrates were covered by conductive tape both on the bottom and top surfaces for SEM examination. Raman characterization was carried out using LabRAM ARAMIS, Horiba Jobin Yvon with a 532 nm wavelength laser. UV-visible spectra were measured by UV-2450 (Shimadzu Co.). The samples for UV characterization were obtained by taking 5 μL suspensions from the vial and then diluting with water. Zeta potentials were collected with a Malvern Zetasizer.

MoS_2 and graphene-based gas sensing

The controlled measurement system consists of five major components: a gas generator, an NH_3 permeation tube, a closed-system sensor cell, and a data acquisition system. We used the 491M gas generator and the NH_3 permeation tube, from Kin-Tek Company (La Marque, TX). At all times, this system was used under a chemical fume hood at room temperature. The NH_3 permeation tube has a calibrated emission rate under controlled temperature. Dry nitrogen was delivered from an ultra-high purity (Grade 5) compressed nitrogen gas cylinder from Airgas. By controlling the rate of emission of ammonia and the nitrogen flow rate, desired concentrations (in ppm range) of ammonia were generated from the gas generator. Before each ammonia exposure test, the NH_3 permeation tube was installed

in the gas generator and heated to a predetermined temperature for around 4 hours in order to obtain a stabilized ammonia concentration. The accuracy of gas concentration output is ±4% according to the calibration results from Kin-Tek. The sensor was installed inside a closed test cell. The concentrated stream of NH_3 was delivered into the test cell *via* a Teflon tube. The MoS_2 or graphene film was placed near the gas inlet port, so that the stream of ammonia was allowed to interact with the sensor surface first.

Results and discussion

Fig. 1 schematically shows the proposed thinning and exfoliation mechanism of combined low-energy ball milling and sonication for the large scale production of 2D nanomaterials. Ball milling can generate two forces on layered materials, namely, shear force and compression force. The shear force can cleave layered materials from their outer surfaces as shown in Fig. 1a, while the compression force peels off thin 2D nanosheets from the edge of layered materials (Fig. 1b). During the thinning process, the low-energy ball milling does not cause significant damage to the in-plane structure of 2D nanosheets and generates fewer defects and impurities, in contrast to sonication.[40] Sonication has been demonstrated as a decent exfoliation procedure in a liquid with a surface tension similar to that of graphite or BN.[41] It is believed that sonication produces a number of effects on exfoliated 2D nanosheets and layered materials: sonication-induced scission that can break larger crystallites into smaller crystallites (Fig. 1c), and the thin 2D nanosheets chipping off from the outer surfaces of layered materials by vibration caused by sonication (Fig. 1d).[41] Then, the 2D nanosheets produced are dispersed in SDS–water solutions. Subsequent centrifugation then removes unexfoliated layered materials and finally stable 2D nanosheet dispersions are successfully obtained in aqueous surfactant solutions.

To demonstrate the thinning effect of combined low-energy ball milling and sonication, firstly we investigate the exfoliation of h-BN at the initial concentration of 10 mg mL^{-1} in a 0.5 mg mL^{-1} surfactant SDS–water solution. Fig. S1a† shows an SEM image of the starting h-BN particles, which have diameters ranging from 0.4 to 1.2 μm. Fig. 2 and S2† show typical characterization results of exfoliated h-BN nanosheets by combined low-energy ball milling and sonication. Fig. 2a is an optical microscopy photograph of milky h-BN dispersion after centrifugation, which has a concentration of up to ~1.2 mg mL^{-1}. To the best of our knowledge, this is the highest concentration reported up to now. The dispersion is stable over periods of hundreds of hours. The zeta potential of the as-prepared BN aqueous dispersion was measured to confirm its stability. The dispersed BN is negatively charged, with a zeta potential of −34.6 mV. The high surface charge ensures that BN nanosheets repel each other in the dispersion, which makes them stable over hundreds of hours. TEM and AFM samples were taken directly from the as-fabricated dispersion, and they contained large quantities of ultrathin 2D nanosheets (Fig. 2b and S2†). Fig. S2† shows the typical AFM image of h-BN nanosheets with sizes ranging from 10 nm to 500 nm and thickness from 1.2 nm to 8 nm. Fig. 2b shows an individual folded h-BN nanosheet and its corresponding selected area electron diffraction (SAED) pattern in Fig. 2c demonstrating that it is monolayer having a six-fold symmetry. By recycling the sediments which were firstly exfoliated by combined lower-energy ball milling and a short duration of sonication and then used as the starting materials for the subsequent exfoliation, the concentration of h-BN nanosheets achieved can be up to 5 mg mL^{-1}. The multiple recycling steps greatly increase the yield of the h-BN exfoliation.[41] Free standing films with thicknesses ranging from nanometres to hundreds of micrometres could be easily fabricated from the high concentration h-BN suspension by vacuum filtration. A typical photograph of a thin h-BN film by vacuum filtration is shown in Fig. S3†. Fig. 2d shows the Raman spectrum from h-BN nanosheets deposited on a Si substrate. In the spectrum, there is one dominant peak at 1367.9 cm^{-1}, which can be assigned to the E_{2g} vibration mode of h-BN. In addition, the UV-visible absorption spectrum of diluted h-BN dispersion was recorded and the result is shown in Fig. 2e. Owing to the low UV cutoff of water as the

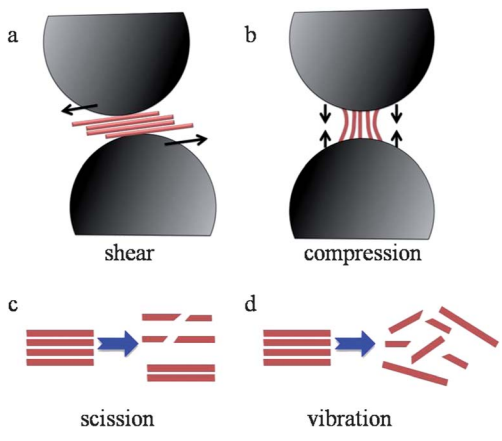

Fig. 1 The illustration of the thinning and exfoliation effects of combined low-energy ball milling and sonication. (a) and (b) 2D nanosheet exfoliation by low-energy ball milling. (a) Shear force-induced exfoliation. (b) Compression force-induced exfoliation. (c) and (d) 2D nanosheet exfoliation by sonication. (c) Sonication-induced scission. (d) Vibration-induced exfoliation.

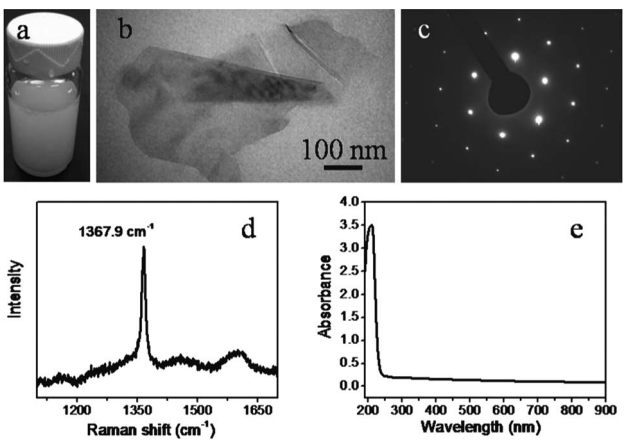

Fig. 2 Exfoliation of layered h-BN by combined low-energy ball milling (12 h) and sonication (2 h) in SDS–water solution. (a) A dispersion of h-BN nanosheets in SDS–water. (b) Typical TEM image of a folded h-BN nanosheet. (c) An SAED pattern of a h-BN nanosheet taken from the right bottom area of (b). (d) Typical Raman spectrum of exfoliated h-BN. (e) An absorption spectrum of diluted h-BN nanosheet dispersion.

solvent, the rather symmetrically shaped band gap peak in the UV-visible absorption spectrum was clearly observed at 207.9 nm, consistent with previous observations.[14,42]

To prove the thinning effect of sonication, control experiments were performed using low-energy ball milling only on h-BN materials. Fig. S4† shows typical TEM images of h-BN nanosheets after milling for various durations (1 h to 12 h) and their corresponding SAED patterns. For samples after 1 h and 3 h milling, large sizes of multi-layer h-BN were still present, and few-layer h-BN nanosheets were barely observed (Fig. S4a and S4b†, respectively). After 6 h (Fig. S4c†) and 12 h (Fig. S4d†) milling, more few-layer and even monolayer h-BN nanosheets were produced. Based on the results of TEM images and SAED patterns, by increasing the milling time from 1 h to 3 h, 6 h, and 12 h, h-BN nanosheets achieved become thinner and smaller. Fig. S5† shows an SEM image of h-BN nanosheets produced by low-energy ball milling for 12 h and then centrifuged at 5000 rpm for 20 minutes. The diameters of these nanosheets range from tens of nanometres to several hundred nanometres. Although an SAED pattern of monolayer h-BN is shown in the inset of Fig. S4d† for 12 h milling sample, we did not get a high yield on exfoliation of layered h-BN by low-energy ball milling only, as per the low yield and low concentration (around 0.1 mg mL^{-1}) of few-layer and monolayer h-BN nanosheets achieved. The above results indicate that additional 2 h sonication is needed for further thinning and exfoliation of layered h-BN materials.

To further verify the thinning and exfoliation effect caused by combined lower-energy ball milling and sonication, we probed other layered materials such as MoS_2 and graphite. Typical exfoliation results of layered MoS_2 and graphite by combined lower-energy ball milling and sonication are shown in Fig. 3 and 4, respectively. Fig. 3a shows an SEM image of starting MoS_2 with diameters of 0.5–10 μm. After ball milling for 12 h and additional 2 h of sonication, the film of MoS_2 nanosheets produced by vacuum filtration is shown in Fig. 3b. In the SEM image, the nanosheets turn transparent under the SEM electron beam due to their small thickness. Deduced from the SEM images in Fig. 3a and b, obviously both the lateral sizes and the thicknesses of layered MoS_2 were reduced by combined lower-energy ball milling and sonication. TEM and AFM were also used to further analyze the structures of MoS_2 nanosheets. Fig. S6† shows a typical AFM image of MoS_2 nanosheets with sizes ranging from 50 nm to 700 nm and thickness from 1.2 nm to 8 nm. Due to their ultrathin shapes, the MoS_2 nanosheets were entirely transparent to the electron beam, as shown in Fig. 3c. Fig. 3d and the inset in Fig. 3c show SAED patterns of four-layer and monolayer MoS_2 nanosheets produced by combined lower-energy ball milling and sonication, respectively. Both patterns reveal a typical six-fold symmetry natural to MoS_2. A typical photograph of MoS_2 suspension is shown in Fig. 3e, and it is found that the dispersion is stable over periods of hundreds of hours. The zeta potential of the as-prepared MoS_2 dispersion is −27.9 mV, which explains its high stability. The concentration of as-fabricated MoS_2 suspension is around a record high ~0.8 mg mL^{-1}. By recycling the sediment as mentioned above, the concentration of MoS_2 nanosheets can increase to 4 mg mL^{-1} and the yield of monolayer MoS_2 nanosheets were greatly enhanced as well. The Raman spectrum of an individual MoS_2 nanosheet is shown in Fig. 3f. It indicates that monolayer or

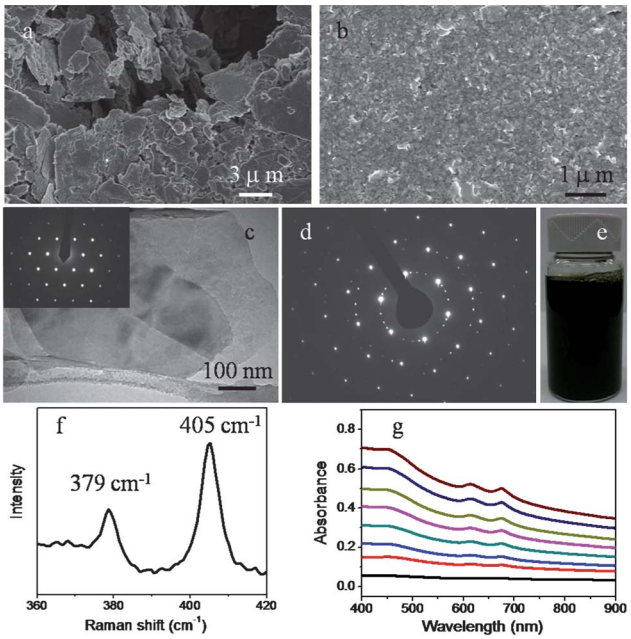

Fig. 3 Exfoliation of layered MoS_2 by combined low-energy ball milling (12 h) and sonication (2 h) in SDS–water solution. (a) and (b) SEM images of MoS_2 before (a) and after (b) the exfoliation, respectively. (c) Typical TEM image of MoS_2 nanosheets. Inset in (c): typical SAED pattern of MoS_2 nanosheets. (d) An SAED pattern of a four-layer MoS_2 nanosheet. (e) A dispersion of MoS_2 nanosheets in SDS–water. (f) Typical Raman spectrum of exfoliated MoS_2. (g) Absorption spectra of diluted MoS_2 nanosheet dispersion. The concentrations are 6.4×10^{-4}, 3.2×10^{-3}, 4.8×10^{-3}, 6.4×10^{-3}, 8.0×10^{-3}, 9.6×10^{-3}, 11.2×10^{-3}, and 12.8×10^{-3} mg mL^{-1}, respectively, increasing from the bottom spectrum to the top one.

bilayer MoS_2 was successfully obtained based on the peak positions of 379 cm^{-1} and 405 cm^{-1}, which are consistent with Raman results of monolayer or bilayer MoS_2 in the literature.[12,43] Fig. 3g shows UV-visible absorption spectra of diluted MoS_2 dispersion. The MoS_2 dispersion exhibited two peaks at 627 nm and 672 nm, which can be attributed to the characteristic A1 and B1 direct excitonic transitions of MoS_2 with the energy split from the valence band spin–orbital coupling.[12] The background is probably due to the light scattering. Both before and after background subtraction, optical absorbance increased with the increase of concentration.

Fig. 4a shows an SEM image of starting graphite materials with diameters of 1–20 μm. After exfoliation by combined lower-energy ball milling and sonication, a high concentration of graphene, ~0.9 mg mL^{-1}, was obtained. The dispersed graphene is negatively charged, with a zeta potential of −23.1 mV, which ensures its stability over hundreds of hours. By recycling the sediment, the concentration of graphene increased to 6 mg mL^{-1}. A photograph of graphene dispersion is shown in Fig. 4e. The dispersion allowed us to prepare graphene films by vacuum filtration. SEM imaging of a thin graphene film shows graphene stacked in-plane in Fig. 4b. Due to their small thickness, graphene nanosheets turn transparent under the SEM electron beam. Fig. 4a and b show typical SEM images of graphite before and after exfoliation by combined lower-energy ball milling and sonication, respectively. It is clear that both the sizes and

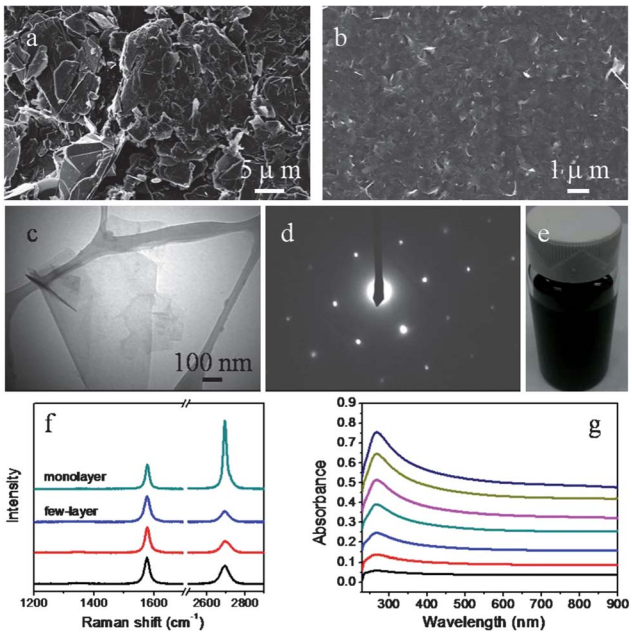

Fig. 4 Exfoliation of graphite by combined low-energy ball milling (12 h) and sonication (2 h) in SDS–water solution. (a) and (b) SEM images of graphite before (a) and after (b) the exfoliation, respectively. (c) Typical TEM image of exfoliated graphene. (d) Typical SAED pattern of exfoliated graphene. (e) A dispersion of exfoliated graphene in SDS–water. (f) Typical Raman spectra of exfoliated graphene. (g) Absorption spectra of exfoliated graphene. The concentrations are 7.2×10^{-4}, 1.8×10^{-3}, 3.6×10^{-3}, 5.4×10^{-3}, 7.2×10^{-3}, 9.0×10^{-3}, and 10.8×10^{-3} mg mL^{-1}, respectively, increasing from the bottom spectrum to the top one.

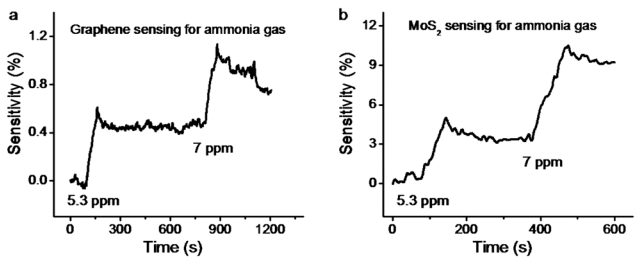

Fig. 5 The sensitivity of graphene (a) and MoS_2-based (b) gas sensing devices toward ammonia.

thicknesses of graphite were reduced. TEM characterizations show a similar result. Graphene nanosheets were transparent to the electron beam shown in Fig. 4c, indicating their small thickness. Fig. 4d shows a typical SAED pattern of monolayer graphene with a six-fold symmetry, where the inner intensity is stronger than the outer intensity. The graphene solution was then deposited on SiO_2 substrates for Raman characterization (Fig. 4f). The Raman spectra show typical monolayer and few-layer graphene characteristics, which are similar to those generally observed for organic solvents exfoliated graphene. Significantly, the low Raman D-band/G-band ratios of <0.05 indicated that lower-energy ball milling and a short duration of sonication cause negligible damage to exfoliated graphene. Optical absorption spectra (Fig. 4g) show features that were expected for exfoliated graphene. The UV-visible spectra exhibits a main absorption peak at 267.8 nm, which can be attributed to the π–π^* transition of C=C bond. In addition, optical absorbance enhanced with the increase of the concentration as shown in Fig. 4g. The above results indicate that using combined lower-energy ball milling and sonication, high concentrations of thin layers of BN, MoS_2, and graphene nanosheets can be successfully obtained in aqueous surfactant solutions. These 2D nanosheets will be ready for large-scale applications.

Large-scale production of 2D nanosheets discussed above, together with their large surface area and strong adsorbability, incite us to investigate their potential application as an ammonia (NH_3) gas sensor. Ammonia is widely used to synthesize various materials in chemical industries. It is a colorless, highly toxic gas with a special odor, is flammable between 16 and 25% by volume, and is very harmful to the human body as it has the potential to harm tissues, affect the immune system, and inhibit growth in cell lines, with 300 ppm IDLH (immediately dangerous to life or health). Therefore, an ammonia sensing system is extremely important to the environment, medical practice, and personnel safety as well as property protection.[44,45] Exfoliated graphene and MoS_2 nanosheets were used to demonstrate their potential application as DC resistor based gas sensors. Graphene and MoS_2 dispersions were deposited on a pre-prepared micro-electrode using a spray coating method. The sensing performance of as-fabricated graphene and MoS_2-based devices was characterized under ambient conditions (*i.e.*, atmospheric pressure and room temperature) against ammonia vapor. As shown in Fig. 5, such graphene and MoS_2-based gas sensors exhibited good sensitivity towards ammonia, which can detect several ppm of ammonia gas. These properties endow 2D nanosheets with great promise as ammonia gas sensors. But further optimization is needed to reduce their recovery time.

Conclusion

In summary, we present a facile, scalable method to fabricate high concentrations of BN, MoS_2, and graphene nanosheets in SDS–water solutions using combined lower-energy ball milling and sonication. The as-fabricated dispersions consist of monolayer and few-layer 2D nanosheets and are relatively stable. These 2D nanosheets were effectively stabilized in SDS–water solutions, which allows us to prepare 2D material papers by vacuum filtration of these 2D dispersions through a membrane filter. Freestanding 2D material papers were acquired by peeling off the membrane after air drying. We also demonstrate that this proposed approach has great potential in the construction of high-performance 2D materials-based devices.

Acknowledgements

The authors would like to acknowledge the financial support from Natural Science Foundation (NSF, 0800849).

References and notes

1 K. S. Novoselov, A. K. Geim, S. V. Morozov, D. Jiang, Y. Zhang, S. V. Dubonos, I. V. Grigorieva and A. A. Firsov, *Science*, 2004, **306**, 666–669.
2 H. Li, Z. Yin, Q. He, H. Li, X. Huang, G. Lu, D. W. H. Fam, A. I. Y. Tok, Q. Zhang and H. Zhang, *Small*, 2012, DOI: 10.1002/smll.201101016.

3 Z. Yin, H. Li, H. Li, L. Jiang, Y. Shi, Y. Sun, G. Lu, Q. Zhang, X. Chen and H. Zhang, *ACS Nano*, 2012, **6**, 74–80.
4 H. Hwang, H. Kim and J. Cho, *Nano Lett.*, 2011, **11**, 4826–4830.
5 A. Splendiani, L. Sun, Y. Zhang, T. Li, J. Kim, C.-Y. Chim, G. Galli and F. Wang, *Nano Lett.*, 2010, **10**, 1271–1275.
6 Z. Zeng, Z. Yin, X. Huang, H. Li, Q. He, G. Lu, F. Boey and H. Zhang, *Angew. Chem., Int. Ed.*, 2011, **50**, 11093–11097.
7 B. Radisavljevic, A. Radenovic, J. Brivio, V. Giacometti and A. Kis, *Nat. Nanotechnol.*, 2011, **6**, 147–150.
8 D. Kim, D. Sun, W. Lu, Z. Cheng, Y. Zhu, D. Le, T. S. Rahman and L. Bartels, *Langmuir*, 2011, **27**, 11650–11653.
9 Y. Yoon, K. Ganapathi and S. Salahuddin, *Nano Lett.*, 2011, **11**, 3768–3773.
10 B. Radisavljevic, M. B. Whitwick and A. Kis, *ACS Nano*, 2011, **5**, 9934–9938.
11 R. J. Smith, P. J. King, M. Lotya, C. Wirtz, U. Khan, S. De, A. O'Neill, G. S. Duesberg, J. C. Grunlan, G. Moriarty, J. Chen, J. Wang, A. I. Minett, V. Nicolosi and J. N. Coleman, *Adv. Mater.*, 2011, **23**, 3944–3948.
12 J. N. Coleman, M. Lotya, A. O'Neill, S. D. Bergin, P. J. King, U. Khan, K. Young, A. Gaucher, S. De, R. J. Smith, I. V. Shvets, S. K. Arora, G. Stanton, H.-Y. Kim, K. Lee, G. T. Kim, G. S. Duesberg, T. Hallam, J. J. Boland, J. J. Wang, J. F. Donegan, J. C. Grunlan, G. Moriarty, A. Shmeliov, R. J. Nicholls, J. M. Perkins, E. M. Grieveson, K. Theuwissen, D. W. McComb, P. D. Nellist and V. Nicolosi, *Science*, 2011, **331**, 568–571.
13 K. K. Kim, A. Hsu, X. Jia, S. M. Kim, Y. Shi, M. Hofmann, D. Nezich, J. F. Rodriguez-Nieva, M. Dresselhaus, T. Palacios and J. Kong, *Nano Lett.*, 2012, **12**, 161–166.
14 Y. Lin, T. V. Williams, T.-B. Xu, W. Cao, H. E. Elsayed-Ali and J. W. Connell, *J. Phys. Chem. C*, 2011, **115**, 2679–2685.
15 T. Terao, C. Zhi, Y. Bando, M. Mitome, C. Tang and D. Golberg, *J. Phys. Chem. C*, 2010, **114**, 4340–4344.
16 A. Nag, K. Raidongia, K. P. S. S. Hembram, R. Datta, U. V. Waghmare and C. N. R. Rao, *ACS Nano*, 2010, **4**, 1539–1544.
17 K. Watanabe, T. Taniguchi and H. Kanda, *Nat. Mater.*, 2004, **3**, 404–409.
18 A. Pakdel, C. Zhi, Y. Bando, T. Nakayama and D. Golberg, *ACS Nano*, 2011, **5**, 6507–6515.
19 Z. Liu, L. Song, S. Zhao, J. Huang, L. Ma, J. Zhang, J. Lou and P. M. Ajayan, *Nano Lett.*, 2011, **11**, 2032–2037.
20 L. Ci, L. Song, C. Jin, D. Jariwala, D. Wu, Y. Li, A. Srivastava, Z. F. Wang, K. Storr, L. Balicas, F. Liu and P. M. Ajayan, *Nat. Mater.*, 2010, **9**, 430–435.
21 V. Leon, M. Quintana, M. A. Herrero, J. L. G. Fierro, A. de la Hoz, M. Prato and E. Vazquez, *Chem. Commun.*, 2011, **47**, 10936–10938.
22 F. Schedin, A. K. Geim, S. V. Morozov, E. W. Hill, P. Blake, M. I. Katsnelson and K. S. Novoselov, *Nat. Mater.*, 2007, **6**, 652–655.
23 J. H. Chen, M. Ishigami, C. Jang, D. R. Hines, M. S. Fuhrer and E. D. Williams, *Adv. Mater.*, 2007, **19**, 3623–3627.
24 Y. M. Lin, K. A. Jenkins, A. Valdes-Garcia, J. P. Small, D. B. Farmer and P. Avouris, *Nano Lett.*, 2009, **9**, 422–426.
25 C. Liu, Z. Yu, D. Neff, A. Zhamu and B. Z. Jang, *Nano Lett.*, 2010, **10**, 4863–4868.
26 Y. Zhu, S. Murali, M. D. Stoller, K. J. Ganesh, W. Cai, P. J. Ferreira, A. Pirkle, R. M. Wallace, K. A. Cychosz, M. Thommes, D. Su, E. A. Stach and R. S. Ruoff, *Science*, 2011, **332**, 1537–1541.
27 A. A. Balandin, S. Ghosh, W. Bao, I. Calizo, D. Teweldebrhan, F. Miao and C. N. Lau, *Nano Lett.*, 2008, **8**, 902–907.
28 K. I. Bolotin, K. J. Sikes, Z. Jiang, M. Klima, G. Fudenberg, J. Hone, P. Kim and H. L. Stormer, *Solid State Commun.*, 2008, **146**, 351–355.
29 C. Lee, X. Wei, J. W. Kysar and J. Hone, *Science*, 2008, **321**, 385–388.
30 M. D. Stoller, S. Park, Y. Zhu, J. An and R. S. Ruoff, *Nano Lett.*, 2008, **8**, 3498–3502.
31 R. Sordan, F. Traversi and V. Russo, *Appl. Phys. Lett.*, 2009, **94**, 073305.
32 S. Stankovich, D. A. Dikin, R. D. Piner, K. A. Kohlhaas, A. Kleinhammes, Y. Jia, Y. Wu, S. T. Nguyen and R. S. Ruoff, *Carbon*, 2007, **45**, 1558–1565.
33 H. Wang, J. T. Robinson, X. Li and H. Dai, *J. Am. Chem. Soc.*, 2009, **131**, 9910–9911.
34 Z. Ding, L. Viculis, J. Nakawatase and R. B. Kaner, *Adv. Mater.*, 2001, **13**, 797–800.
35 H. S. S. Ramakrishna Matte, A. Gomathi, A. K. Manna, D. J. Late, R. Datta, S. K. Pati and C. N. R. Rao, *Angew. Chem., Int. Ed.*, 2010, **49**, 4059–4062.
36 D. Yang and R. F. Frindt, *J. Phys. Chem. Solids*, 1996, **57**, 1113–1116.
37 P. Joensen, R. F. Frindt and S. R. Morrison, *Mater. Res. Bull.*, 1986, **21**, 457–461.
38 M. B. Dines, *J. Chem. Educ.*, 1974, **51**, 221.
39 K.-G. Zhou, N.-N. Mao, H.-X. Wang, Y. Peng and H.-L. Zhang, *Angew. Chem., Int. Ed.*, 2011, **50**, 10839–10842.
40 W. Zhao, F. Wu, H. Wu and G. Chen, *J. Nanomater.*, 2010, **2010**, 528235.
41 U. Khan, H. Porwal, A. O'Neill, K. Nawaz, P. May and J. N. Coleman, *Langmuir*, 2011, **27**, 9077–9082.
42 Y. Lin, T. V. Williams and J. W. Connell, *J. Phys. Chem. Lett.*, 2010, **1**, 277–283.
43 C. Lee, H. Yan, L. E. Brus, T. F. Heinz, J. Hone and S. Ryu, *ACS Nano*, 2010, **4**, 2695–2700.
44 H. Bai and G. Shi, *Sensors*, 2007, **7**, 267–307.
45 E. Bekyarova, M. Davis, T. Burch, M. E. Itkis, B. Zhao, S. Sunshine and R. C. Haddon, *J. Phys. Chem. B*, 2004, **108**, 19717–19720.